Spontaneous Exfoliation of Single-Walled Carbon Nanotubes Dispersed Using a Designed Amphiphilic Peptide

ARTICLE *in* BIOMACROMOLECULES · MARCH 2008

Impact Factor: 5.75 · DOI: 10.1021/bm701181j · Source: PubMed

6 AUTHORS, INCLUDING:

Helen Fox (née Cathcart)
Waterford Institute of Technology
6 PUBLICATIONS **253** CITATIONS
SEE PROFILE

Alan B Dalton
University of Surrey
119 PUBLICATIONS **5,149** CITATIONS
SEE PROFILE

Gregg R Dieckmann
University of Texas at Dallas
35 PUBLICATIONS **2,141** CITATIONS
SEE PROFILE

Jonathan Coleman
Trinity College Dublin
192 PUBLICATIONS **15,278** CITATIONS
SEE PROFILE

Spontaneous Exfoliation of Single-Walled Carbon Nanotubes Dispersed Using a Designed Amphiphilic Peptide

Valeria Nicolosi,[†] Helen Cathcart,[†] Alan R. Dalton,[‡] Damian Aherne,[§] Gregg R. Dieckmann,[△] and Jonathan N. Coleman*[,†,⊥]

School of Physics, Trinity College Dublin, Dublin 2, Ireland, School of Electronics & Physical Sciences, University of Surrey, Surrey GU2 7XH, United Kingdom, School of Chemistry, Trinity College Dublin, Dublin 2, Ireland, Chemistry Department and Alan G. MacDiarmid NanoTech Institute, The University of Texas at Dallas, Richardson, Texas, and Centre for Research on Adaptive Nanostructures and Nanodevices (CRANN), Trinity College Dublin, University of Dublin, Dublin 2, Ireland

Received October 25, 2007; Revised Manuscript Received December 11, 2007

We have observed concentration dependent exfoliation of single-walled carbon nanotubes dispersed in solutions of the synthetic peptide nano-1. As the nanotube concentration is reduced, the bundle diameters tend to decrease before saturating at <2.0 nm for concentrations below 6×10^{-3} mg/mL. The fraction of individual nanotubes increases with decreasing concentration, saturating at ~95% at low concentration. This concentration dependent exfoliation happens even if the dispersions are not sonicated on dilution, albeit over a longer time scale. The populations both of individual nanotubes and of bundles are much higher than expected at high concentrations, indicating the presence of repulsive internanotube interactions stabilizing the dispersions.

To take full advantage of the unsurpassed physical properties of carbon nanotubes, it is generally necessary to have access to individualized nanotubes. However, due to their high surface energy,[1] nanotubes tend to agglomerate in ropes or bundles, which can be tens of nanometers wide and many micrometers long. Exfoliating nanotubes from these bundles is a nontrivial task that usually requires dispersion in a liquid medium and significant energy input.

In the past, single-walled carbon nanotubes (SWNTs) have generally been dispersed in water with the aid of surfactants such as sodium dodecyl sulfate.[2] Alternatively, single-stranded DNA has been used to individually disperse nanotubes[3] and even separate nanotubes by electronic type.[4] More recently, designed synthetic peptides have proven effective at dispersing and individualizing nanotubes.[5,6] One class of peptides has been carefully designed to fold into α-helical secondary structures, with one side displaying hydrophobic residues capable of interacting with nanotubes surfaces and the other side containing hydrophilic groups that interact strongly with water.[5,7] Using these peptides, high quality dispersions can be produced with very little sonication, minimizing damage to the nanotubes. More importantly, these peptides are useful because not only can they individualize SWNTs with high yield, but also because their structure can be varied,[8] allowing the control of interpeptide interactions, leading to self-assembly of peptide-coated SWNTs into hierarchical structures.[9] In addition, coating with carefully selected peptides potentially allows the deposition of nanotubes at defined regions of cells or other biological entities.

Of all the criteria for good dispersions, one is paramount: the yield (i.e., number fraction) of individual nanotubes should be maximized. This should occur at as high a concentration as possible, leading to a high number density of individual nanotubes. In most cases, the preparation of individual dispersed SWNTs is achieved through ultracentrifugation (UCF) of primary surfactant or biomolecule stabilized dispersions. This results in the removal of bundles and large aggregates. If the UCF conditions are optimized, this should lead to a high yield of individual nanotubes at high concentration. However, recent work on dispersions of SWNTs in DNA has demonstrated that similar results can be achieved by dilution rather than ultracentrifugation.[10] This process works because SWNTs tend to arrange themselves in bundles whose diameter distribution is concentration dependent.[10,11] Dilution tends to shift the bundle diameter distribution to lower values, mimicking the removal of larger bundles. This procedure has two significant advantages: the loss of nanotubes associated with ultracentrifugation can be avoided, and both diameter distribution and population of individual nanotubes can be optimized by careful choice of concentration.[10,11] Thus, concentration control offers a means to further enhance the ability of synthetic peptides to disperse and exfoliate nanotubes. In addition, we expect quantitative studies to shed light on the mechanisms of nanotube dispersion.

In this work, we study the effect of dilution on dispersions of nanotubes in peptide/water solutions. At medium to high concentrations, individual nanotubes and small bundles coexist with large nanotube aggregates, which can be removed by mild centrifugation. At lower concentrations, only individual nanotubes and small bundles are observed. We demonstrate exfoliation of nanotubes from bundles as the concentration is reduced. At concentrations below $\sim 10^{-2}$ mg/mL, the nanotube:bundle ratio exceeds 10:1. Detailed analysis shows that, even at high concentration, significant populations of individual nanotubes exist. The high number density of individual nanotubes and small bundles at high concentration can only be explained by stabilization by electrostatic repulsion.

The peptide used in this work is a synthetic, 29-residue peptide, synthesized in-house and denoted nano-1. It has been

* Corresponding author. E-mail: colemaj@tcd.ie.
[†] School of Physics, Trinity College Dublin.
[‡] School of Electronics & Physical Sciences, University of Surrey.
[§] School of Chemistry, Trinity College Dublin.
[△] Chemistry Department and NanoTech Institute, The University of Texas at Dallas.
[⊥] Centre for Research on Adaptive Nanostructures and Nanodevices (CRANN), Trinity College Dublin, University of Dublin.

10.1021/bm701181j CCC: $40.75
Published on Web 01/26/2008

described in more detail elsewhere.[7] Its sequence is Ac-Glu-Val-Glu-Ala-Phe-Glu-Lys-Lys-Val-Ala-Ala-Phe-Glu-Ser-Lys-Val-Gln-Ala-Phe-Glu-Lys-Lys-Val-Glu-Ala-Phe-Glu-His-Gly-$CONH_2$. Purified SWNTs were purchased from Carbon Nanotechnologies, Inc. and used as supplied. All nanotube−peptide dispersions were prepared from a common high concentration stock dispersion. This was prepared by sonicating purified HiPco SWNTs (1 mg/mL) and peptide (3 mg/mL) in deionized water by using a high power ultrasonic tip processor, model GEX600 (60 W, 60 kHz) for 2 min. This stock dispersion was split in two and two dilution series prepared by successive dilution with water down to $\sim 10^{-3}$ mg/mL SWNTs. In one series, the dispersions were sonicated after every dilution (2 min, 60 W), while in the other series, no sonication was applied. After dilution, each dispersion was allowed to equilibrate for an hour before measurement of its UV–vis−NIR absorption spectrum with a Perkin-Elmer Lambda 900 UV–vis−NIR spectrometer. At this stage, small aggregates ($\sim 100\ \mu$m in size) could be observed in the higher concentration samples. These aggregates were removed from each dispersion by mild centrifugation (CF) at 5500 rpm ($\sim 2700\ g$) for 90 min using a Hettich EBA-12 centrifuge. After CF, the UV–vis−NIR spectrum was remeasured for each dispersion. Comparison of the before and after CF spectra allowed us to calculate the fraction of material removed during CF as well as the true concentration after CF. After CF, a drop of each dispersion was placed on a mica substrate and allowed to dry in ambient conditions. AFM measurements were made on each sample using a DI Multimode Nanoscope IIIA. It is known from previous studies of this kind on SWNT dispersions that SWNT aggregation on the substrate is minimal.[10,11] Thus we believe that the AFM measurements represent the state of the dispersion in situ. Point-probe silicon nitride cantilevers (force constant = 42 Nm^{-1}, resonant frequency = 330 kHz) were used for all measurements. In addition, AFM measurements were made on the nonsonicated samples four weeks after sample prep. Zeta potential measurements were performed using a Malvern Zetasizer Nano.

Absorption spectra (see Supporting Information) measured for both sonicated and nonsonicated samples displayed van Hove singularities typical of well-dispersed nanotubes.[10,11] The absorbance ($\lambda = 660$ nm) divided by cell length (A/l) is plotted as a function of initial nanotube concentration, C_i, for the nonsonicated samples both before and after CF in figure 1. The results for the sonicated samples (not shown) were very similar. Before CF, in spite of the presence of large aggregates at higher concentrations, A/l scaled linearly with concentration over the whole concentration range for both the sonicated and nonsonicated samples, allowing the calculation of the nanotube absorption coefficients to be 1737 and 1696 mL/(mg m), respectively. After CF, for both sample types, A/l initially increased linearly with concentration before falling off at concentrations above 10^{-2} mg/mL. This is indicative of the removal of aggregates by CF at higher concentrations.[11] The fraction of nanotube material contained in the aggregates, χ_{agg}, can be calculated from the absorbance before and after CF[11] and is plotted versus initial nanotube concentration C_i in figure 1b. It is clear that virtually no aggregates form at lower concentrations while the majority of the nanotubes aggregate at concentrations above 5×10^{-2} mg/mL. Crossed polarized microscopy and SEM measurements (not shown) revealed that the aggregates consisted of amorphous agglomerates of nanotube bundles with no internal ordering or alignment as observed in other systems.[12]

After centrifugation, the dispersions consist only of dispersed nanotubes with all the aggregates having been removed by CF.

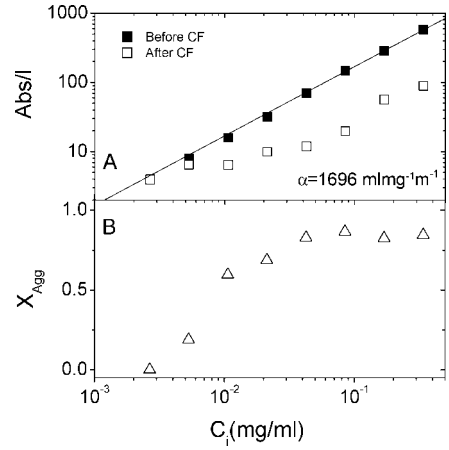

Figure 1. (A) Absorbance per unit length ($\lambda = 660$ nm) for nonsonicated peptide−nanotube dispersions as a function of initial nanotube concentration C_i before and after centrifugation (2700*g*, 90 min). At this wavelength, the absorbance is dominated by the nanotube absorption. The solid line is a fit to the Lambert–Beer law. (B) Mass fraction of nanotube aggregates as a function of initial nanotube concentration. This is found from the absorbance data shown in (A): $(A_B - A_A)/A_B$, where the subscripts B and A denote before and after centrifugation, respectively.

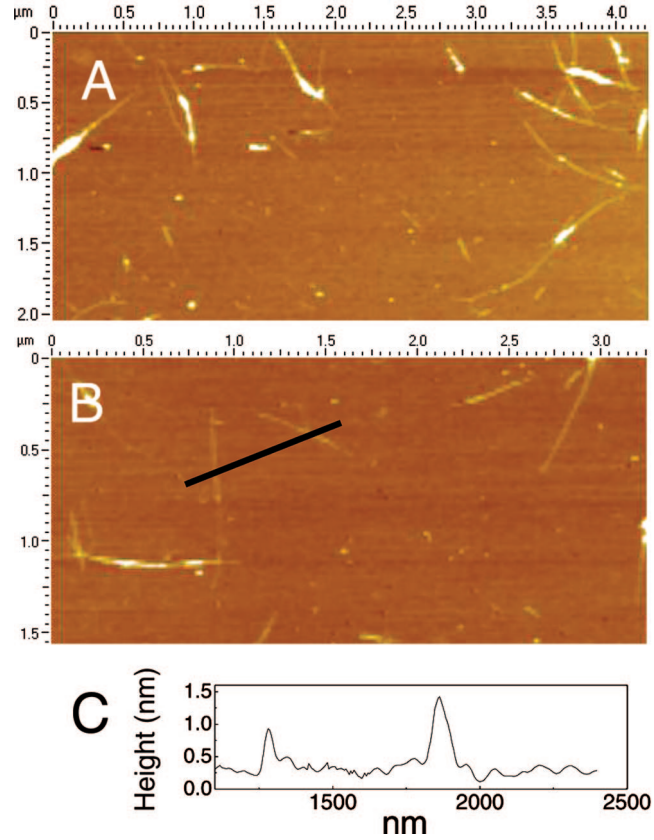

Figure 2. AFM images of nanotubes and bundles deposited on mica from (A) a high concentration (0.033 mg/mL) dispersion and (B) a low concentration (0.0031 mg/mL) dispersion. (C) Height profile for the two nanotubes illustrated in (B).

The actual concentration of nanotubes after CF, C_{NT}, can be found from: $C_{NT} = C_i(1 - \chi_{Agg})$. To investigate the state of the dispersion after CF, AFM measurements were made for each sample. In all cases, large numbers of rodlike objects (see Figure 2a, b) were observed with diameters and lengths ranging up to 13 nm and 4 μm, respectively. As SWNTs have diameters in the 1 nm range, this shows that many of the dispersed objects

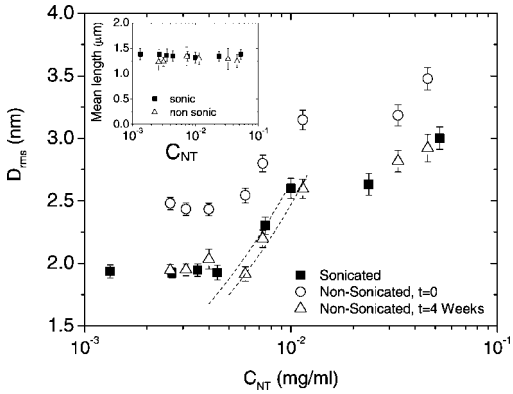

Figure 3. Root-mean-square diameter distributions for nanotube bundles (including individual nanotubes) stabilized by nano-1 as a function of nanotube concentration. Shown are data for samples prepared by sonication after every dilution (black squares). Also shown are data for samples diluted without sonication measured both immediately after dilution (circles) and four weeks after dilution (triangles). The dashed lines are fits to eq 1. Inset: mean bundle length as a function of concentration for both sonicated and nonsonicated samples.

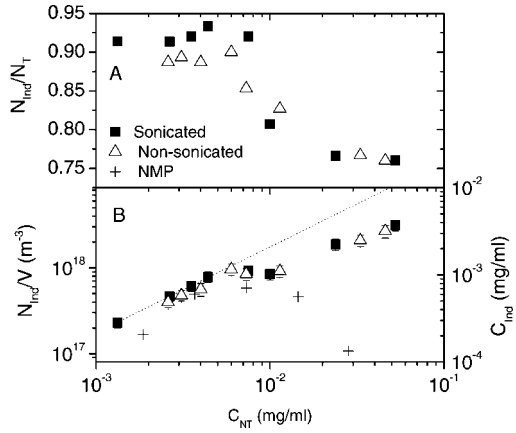

Figure 4. Population of individual nanotubes as a function of nanotube concentration. An individual nanotube is defined rather arbitrarily as an object of height <3 nm to take into account the peptide coating. In both cases, data is presented for both sonicated and nonsonicated samples. (A) Number of individual nanotubes as a fraction of the total number of 1D objects observed by AFM. (B) Number density of individual nanotubes as a function of nanotube concentration. Shown on the right axis is the concentration of individual nanotubes calculated using an average nanotube molar mass of 700 kg/mol (ref 11). Note that the number density of individual nanotubes initially decreases with decreasing concentration, unlike the situation for nanotubes dispersed in NMP (represented by +). In addition, the number density does not deviate as strongly from the trend expected in the absence of concentration dependent exfoliation (dashed lines).

are bundles. As it is known that bundle size scales with concentration in a number of systems,[10,11,13] we measured the root-mean-square rod diameter, D_{rms}, for each sample. Data for D_{rms} as a function of C_{NT} is shown for the sonicated samples in figure 3 (black squares). The root-mean-square diameter falls steadily from ~3 nm before saturating at <2 nm for concentrations below 5×10^{-3} mg/mL. Such debundling has been observed previously for a number of systems, including SWNTs dispersed using genomic DNA.[10]

It is generally considered that nanotube exfoliation requires energy input in the form of sonication.[14] However, spontaneous debundling of nanowires in isopropyl alcohol[15] and nanotubes dispersed using DNA has been observed.[10] To test the possibility that this might occur in SWNT-nano-1 dispersions, AFM measurements were made on a dilution series produced without sonication. Shown in figure 3 (open circles) are D_{rms} measurements made on samples deposited shortly after dilution. While a decrease in bundle diameter with decreasing concentration is observed, it is by no means as pronounced as for the sonicated samples, saturating at 2.5 nm at low concentration. However, exfoliation in the absence of ultrasound is likely to be a slow process, so the data just discussed likely reflect dispersions that are far from equilibrium. To test this, AFM measurements were repeated for samples deposited four weeks after dilution. This data (open triangles in figure 3) match the data for the sonicated samples very closely, suggesting that a concentration dependent equilibrium exists and sonication acts only to accelerate the kinetics.

Previous studies on dispersion of nanotubes in the solvent *N*-methyl-pyrrolidone[11] have shown that the concentration dependence of D_{rms} (above saturation) can be described by:

$$D_{rms} = \sqrt{\langle D^2 \rangle} \approx \left[\frac{4C_{NT}}{\rho_{NT} \pi L (N/V)_{Eq}} \right]^{1/2} \quad (1)$$

where L is the mean length of all observed objects, bundles, and individual nanotubes. This equation describes a model where the nanotubes arrange themselves in bundles such that the number density of bundles (and individual nanotubes) $(N/V)_{Eq}$ is concentration independent. This equation has been fitted to both the sonicated and nonsonicated equilibrium data in Figure 3. In both cases, the data only fit the model over a very small concentration range, with D_{rms} increasing with concentration much slower than expected above $C_{NT} = 0.01$ mg/mL.

In the concentration range where the model fits the data, the equilibrium number density of bundles (and individuals)[11] can be calculated if the average length is known. The average length of all bundles and individuals was measured from the AFM data at a range of concentrations for both the sonicated and nonsonicated equilibrium samples. The average lengths were equal within error at all concentrations (figure 3 inset), giving average values of 1.2 ± 0.1 and 1.3 ± 0.1 μm, respectively. Knowledge of these mean lengths allows us to calculate $(N/V)_{Eq}$ from the fits to eq 1, giving values of 1.0×10^{18} and 1.1×10^{18} m^{-3} for the sonicated and nonsonicated samples, respectively. For similar SWNTs dispersed in NMP,[11] $(N/V)_{Eq} = 1.5 \times 10^{18}$ m^{-3}, equivalent to each bundle/individual, on average occupying a volume of solvent approximately equal to the sphere whose diameter is equal to the mean bundle/individual length.[11] In this arrangement, the dispersed rods are stable against collisional aggregation due to diffusive rotation. Taking into account the measured average rod lengths, we calculate that for both sonicated and nonsonicated samples measured here, we are very close to this condition in the concentration range between 4×10^{-3} and 10^{-2} mg/mL.

Another metric for nanotube exfoliation is to track the population of individual nanotubes as a function of concentration. We can do this by counting all objects observed in the AFM that have a diameter less than some cutoff. In this work, we need to take into account the nanotube diameter including peptide coating. We can estimate this diameter from HRTEM and modeling to be ~3 nm,[9] although we recognize that the coating is unlikely to be regular, making this figure somewhat arbitrary. This allows us to estimate the fraction of individual nanotubes, N_{ind}/N_t, which is plotted as a function of nanotube concentration in figure 4a. Even at high concentration, 75% of the objects can be classified as individual nanotubes in nano-1 dispersions, much higher than the 5% at equivalent concentra-

tions of SWNTs in NMP.[11] As the concentration is reduced, this figure increases before saturating at ~95%, a figure superior to any other dispersant recorded.

We can use this data to calculate the number density of individual nanotubes,[11] N_{ind}/V, which is plotted in Figure 4b as a function of C_{NT}. If nanotubes existed solely as individual nanotubes, or if the fraction of individual nanotubes is constant, as is the case at low concentration (Figure 4a), then N_{ind}/V will scale linearly with C_{NT}, as shown by the dotted line in figure 4b. The presence of concentration dependent bundling, however, tends to cause this curve to turn over and even decrease as concentration is increased (the equivalent curve for SWNTs in NMP is shown for comparison). Such a turnover is observed in the concentration range between 4×10^{-3} and 10^{-2} mg/mL in Figure 4b. However, at concentrations above 10^{-2} mg/mL, N_{ind}/V begins to increase again, albeit in a sublinear fashion. This has not been observed in other systems.[10,11,13] It should be pointed out that this increase occurs over the same concentration range as the slower than expected increase in D_{rms} with C_{NT} shown in Figure 3 ($C_{NT} > 10^{-2}$ mg/mL).

To investigate this further, we calculate the number of rods (bundles and individuals), N_{sphere}, which exist on average, at equilibrium, in each spherical volume defined by the average bundle (including individual) length:

$$N_{sphere} = \frac{N_{Tot}}{V}\frac{4}{3}\pi\left(\frac{L}{2}\right)^3 = \frac{4C_{NT}}{\rho_{NT}\pi D_{rms}^2 L}\frac{4}{3}\pi\left(\frac{L}{2}\right)^3 = \frac{2C_{NT}L^2}{3\rho_{NT}D_{rms}^2} \quad (2)$$

where N_{Tot}/V is the concentration-dependent rod number density (N_{Tot}/V is equal to $(N/V)_{Eq}$ over the narrow concentration range where eq 1 is a good fit to the data.). N_{sphere} is plotted as a function of nanotube concentration in Figure 5. This data resembles that presented in Figure 4b, showing that the concentration dependence of N_{tot}/V resembles that of N_{Ind}/V, as would be expected as the sample is predominately individual nanotubes. Both sonicated and nonsonicated data are very similar, with both data sets having three definite regimes. At low concentrations ($C_{NT} < 5 \times 10^{-3}$ mg/mL), N_{sphere} is less than one and scales linearly with concentration. This is the regime where ~95% of objects observed in the AFM are individual nanotubes and which can be considered dilute. In this regime, as C_{NT} increases, the nanotubes tend to get closer together, resulting in an increase in N_{Sphere}. At intermediate concentrations (5×10^{-3} mg/mL $< C_{NT} < 1.4 \times 10^{-2}$ mg/mL), N_{sphere} is constant. This reflects the regime where eq 1 fits the D_{rms} data well, i.e., the regime where there is a concentration independent bundle number density. For SWNTs in NMP and other systems in the literature, this regime extends to all concentrations measured above saturation.[11,13] That N_{sphere} is very close to 1 in this region shows that peptide-coated nanotubes/bundles tend to exist stably in a volume of solvent given by the sphere traced by their tips as observed previously for SWNTs in NMP.[11] We have labeled this region with the term volume stabilized. At higher concentrations ($C_{NT} > 1.4 \times 10^{-2}$ mg/mL), N_{sphere} begins to increase again. In this region, the bundles/individuals exist in very close proximity, yet aggregation at these concentrations is minimal, as reflected by the weak increase in D_{rms} observed in Figure 3. By a concentration of 4×10^{-2} mg/mL, on average four rods exist per spherical volume. It should be pointed out that the same results are observed for the sonicated samples and the nonsonicated samples that have been undisturbed for four weeks, indicating that this situation is stable.

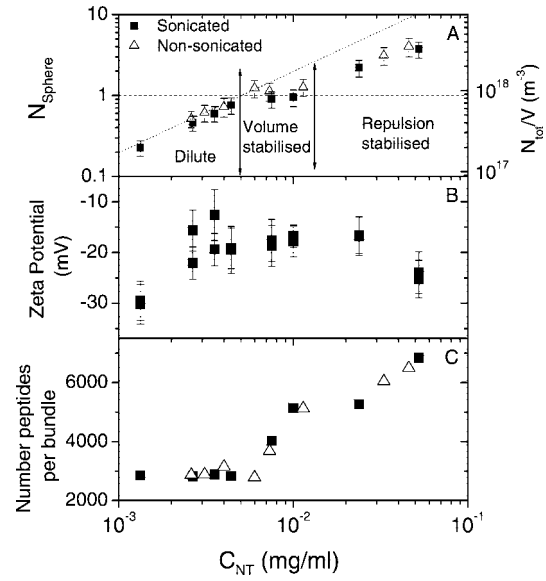

Figure 5. (A) Number of bundles (including individual nanotubes) per spherical volume defined by the average bundle length. In the low concentration regime (labeled dilute), the bundles are far apart. In the intermediate regime, on average each bundle occupies a volume equal to the volume of the sphere traced out by its ends. In the high concentration regime, more than one bundle occupies its own spherical volume, suggesting that the peptide-coated bundles are coated by interpeptide repulsive interactions. Shown on the right axis is the number of bundles per unit volume. This scale is approximate, as the mean bundle length is different for the sonicated and nonsonicated samples. (B) Zeta potential as a function of nanotube concentration. (C) Number of peptides per bundle as a function of nanotube concentration as calculated from eq 3.

For a number of rods significantly greater than 1 to coexist stably in a given spherical volume, the rods must somehow be stabilized against aggregation. Otherwise, diffusive rotation will eventually result in adjacent nanotubes/bundles coming into contact and aggregating. The most likely cause of this stabilization is electrostatic repulsion. Computer simulation has shown that, for a typical (8,8) nanotube, approximately six nano-1 α-helices can surround the nanotube circumference.[7] Nano-1 has been designed such that, when folded into an α-helix, hydrophobic residues along one side of the helix are available to interact with the nanotube surface. Adjacent helices are stabilized by complementary polar residues. The outer face of the peptide coating contains polar residues to facilitate interactions with the solvent (water). Identical polar residues on nearby SWNT−peptide complexes could repel each other over short−medium length scales. Our results suggest that when averaged over all surface−residue pairs, the net effect of the inter-SWNT−peptide interactions is repulsive, resulting in the stabilization of dispersed complexes. Such stabilization has previously been observed for acid-based SWNT dispersions, where up to ~30 protonated individual nanotubes were observed per spherical volume.[16]

Such electrostatic repulsion is generally quantified by the electrical potential in the vicinity of the surface of the complex. In colloidal science, this potential is known as the zeta potential (ζ). A charged colloidal particle will generally be surrounded by a tightly bound layer of counterions which, in turn, is surrounded by a more diffuse zone of mobile counterions. The ζ potential is the potential at the edge of the region of bound counterions. As pristine carbon nanotubes themselves are nonpolar, they tend to have a ζ potential very close to zero in neutral solutions (pH ~ 7).[2] However, when coated with peptide,

it is likely that the nanotube−peptide hybrid has a nonzero ζ potential due to ionization of the glutamic acid and lysine amino acid side chains in nano-1. Measurements of the ζ potential were made for the nano-1 and for the composite dispersions at each concentration studied (Figure S2, Supporting Information). For the nano-1, a strong peak was observed at −42 mV. For the composites in general, the ζ trace showed one peak only, although for some lower concentrations, a small shoulder was observed around −40 mV. We tentatively attribute this to an equilibrium population of unbound peptide at low concentration. We expect the fraction of unbound peptide to decrease with increasing population,[17] as evidenced by the disappearance of the peak at −40 mV at higher concentrations. The ζ potentials (measured from the peak positions) of the sonicated dispersions are shown in Figure 5b and vary between −24 and −12.6 mV. For comparison purposes, we measured the ζ potential of SWNT dispersed using DNA[10] at a nanotube concentration of 0.014 mg/mL to be −38 mV, significantly more negative than for these peptide-based samples. Interestingly, the ζ potential data can be divided into the same three concentration ranges as the N_{sphere} data. At low concentrations ($C_{NT} < 5 \times 10^{-3}$ mg/mL), ζ increases from −30 to −13 mV. At intermediate concentrations (5×10^{-3} mg/mL $< C_{NT} < 1.4 \times 10^{-2}$ mg/mL), ζ is constant, while for concentrations above 1.4×10^{-2} mg/mL, ζ appears to decrease again. This is interesting, as this is exactly the concentration range where we see N_{sphere} increase above 1. Thus, it is clear that the large values of N_{sphere} and the anomalously high rod number density observed may be due to increases in the absolute value of the ζ potential at high concentration. These increased values of |ζ| must be the result of each peptide-coated bundle carrying a greater charge at higher concentrations. The simplest explanation for this is that there are more adsorbed peptides per bundle at higher concentrations.

To explore this, we consider the total number of peptides per bundle. This quantity tends to increase as nanotube aggregation proceeds and is given by:

$$\frac{N_{Peptide}}{N_{Tot}} = \frac{C_{Peptide}}{M_{peptide}} \frac{\rho_{NT} \pi D_{rms}^2 L}{4 C_{NT}} \quad (3)$$

where $M_{peptide}$ is the peptide molecular mass (3354 g/mol). This quantity has been calculated from the D_{rms} data and is plotted in Figure 5C. At low concentrations, the number of peptides per bundle is constant as, in the absence of nanotube aggregation, numbers of both peptides and bundles increase linearly with concentration. However, above 5×10^{-3} mg/mL, aggregation begins to occur, resulting in a large increase in the number of peptides per bundle (aggregation can occur in this concentration range due to the fact that |ζ| < 30 mV). In terms of ζ potential, a more relevant quantity is the number of *bound* peptides per bundle. For systems such as these where the dispersant is reversibly bound to the nanotube, the fraction of bound peptides increases with increasing concentration,[17] resulting in an increase in bound peptides per bundle even more rapid than that shown in Figure 5C. This increase in bound peptide per bundle leads to an decrease in ζ potential (i.e., ζ gets more negative), as shown for the high concentration regime in Figure 5B. This results in a slowdown in aggregation, resulting in large quantities of small bundles at high concentration, leading to surprisingly high values of N_{sphere}.

Finally, we note that these dispersions are not indefinitely stable. After 3–4 months, aggregates begin to appear. This is an intriguing but poorly understood phenomenon. For example, if freshly prepared, high concentration dispersion is diluted and then allowed to stand undisturbed, the bundles will exfoliate over a period of four weeks. However, over the next 8–12 weeks, the nanotubes reaggregate to form large agglomerates, visible to the naked eye. One possible cause of this reaggregation process is a slow desorption of peptide from the nanotubes over time, resulting in large quantities of free peptide but only small quantities of bound peptide. Eventually, the reduced quantities of bound peptide will no longer be enough to stabilize the nanotubes, resulting in aggregation. This has previously been observed over shorter timescales for nanotube−surfactant dispersions after dilution with water.[18] However, this explanation sheds no light on the initial exfoliation mechanism, which remains a mystery.

In conclusion, we have demonstrated efficient exfoliation of nanotubes in low concentration synthetic peptide dispersions. Root-mean-square bundle diameters of 2 nm are observed at concentrations below 6×10^{-3} mg/mL. At these concentrations, up to 95% of objects observed had dimensions commensurate with individual nanotubes. Unlike other dispersions based on solvents, large populations of nanotubes were observed at high concentrations. In fact, the proximity of dispersed bundles was much higher than expected in the higher concentration range, with up to four bundles occupying each sphere based on the bundle length. These systems are stabilized through interpeptide repulsions, as evidenced by high |ζ| at high concentrations.

Acknowledgment. We would like to thank Jane H. Nguyen and Eric J. Becraft for preparation of nano-1. This work was supported by a grant from the Human Frontier Science Program (JNC, ABD, GRD; grant RGY0070/2005-C).

Supporting Information Available. Absorption spectra for the $C_{NT} = 0.023$ mg/mL dispersion before and after centrifugation. Zeta potential curves for Nano-1 and the composite dispersions for each nanotube concentration. This material is available free of charge on the Internet at http://pubs.acs.org.

References and Notes

(1) Nuriel, S.; Liu, L.; Barber, A.; Wagner, H. D. *Chem. Phys. Lett.* **2005**, *404*, 263.
(2) O'Connell, M. J. *Science* **2002**, *297*, 593.
(3) Zheng, M. *Nat. Mater.* **2003**, *2*, 338.
(4) Zheng, M. *Science* **2003**, *302*, 1545.
(5) Arnold, M. S.; Guler, M. O.; Hersam, M. C.; Stupp, S. I. *Langmuir* **2005**, *21*, 4705.
(6) Witus, L. S. *J. Mater. Chem.* **2007**, *17*, 1909.
(7) Dieckmann, G. R. *J. Am. Chem. Soc.* **2003**, *125*, 1770.
(8) Zorbas, V. *J. Am. Chem. Soc.* **2005**, *127*, 12323.
(9) Dalton, A. B. *Adv. Funct. Mater.* **2004**, *14*, 1147.
(10) Cathcart, H. *J. Phys. Chem. C* **2007**, *111*, 66.
(11) Giordani, S. *J. Phys. Chem. B* **2006**, *110*, 15708.
(12) Bergin, S. D., et al. **2007**, submitted.
(13) Nicolosi, V.; Vengust, D.; Mihailovic, D.; Blau, W. J.; Coleman, J. N. *Chem. Phys. Lett.* **2006**, *425*, 89.
(14) Strano, M. S. *J. Nanosci. Nanotechnol.* **2003**, *3*, 81.
(15) Nicolosi, V. *Eur. Phys. J.: Appl. Phys.* **2007**, *37*, 149.
(16) Davis, V. A. *Macromolecules* **2004**, *37*, 154.
(17) Coleman, J. N. *J. Phys. Chem. B* **2004**, *108*, 3446.
(18) McDonald, T. J.; Engtrakul, C.; Jones, M.; Rumbles, G.; Heben, M. J. *J. Phys. Chem. B* **2006**, *110*, 25339.

BM701181J